Convergent close-coupling method for the calculation of electron scattering on hydrogenlike targets

Igor Bray*
Electronic Structure of Materials Centre, The Flinders University of South Australia, G.P.O. Box 2100, Adelaide 5001, Australia
(Received 10 September 1993)

We extend the convergent close-coupling method for the calculation of electron-hydrogen scattering to hydrogenlike targets, atoms, or ions. These include H, Li, Na, and K atoms, as well as the multitude of ions which have the same isoelectronic sequence as any of these atoms. The reliability of the method is independent of the projectile energy, and we demonstrate its applicability by achieving excellent agreement with a large set of measurements for electron scattering on sodium at projectile energies ranging from 1 to 54.4 eV. These measurements include spin asymmetries, singlet and triplet $L_\perp$, reduced Stokes parameters, differential, integrated, and total cross sections, as well as the total ionization spin asymmetry. The method is found to give better agreement with experiment than any other over this entire energy range.

PACS number(s): 34.80.Bm, 34.80.Dp, 34.80.Kw, 34.80.Nz

I. INTRODUCTION

Calculation of electron-atom or electron-ion scattering is of both fundamental and practical interest to physicists. The simplest system, electron scattering on atomic hydrogen, is difficult to calculate and there still exist discrepancies between theory and experiment; see Bray and Stelbovics [1], for example. It is for this reason that this system has attracted so much attention. The discrepancies with the angular correlation parameters in the intermediate energy range have resulted in the development of some of the most sophisticated electron-atom scattering theories such as the intermediate-energy R-matrix method of Scholz *et al.* [2], the pseudo-state methods of Callaway [3] and van Wyngaarden and Walters [4], the second-order distorted-wave theory of Madison, Bray, and McCarthy [5], the coupled-channel optical (CCO) method of Bray, Konovalov, and McCarthy [6], and the convergent close-coupling (CCC) method of Bray and Stelbovics [1]. These methods all tend to agree much more with each other than with experiment.

The development of the CCC method for hydrogen has taken the close-coupling formalism to completeness. The method is without approximation, but relies on being able to achieve convergence in the observable of interest as a function of the number of states in the multichannel expansion. These states are obtained by diagonalizing the target Hamiltonian in a large Laguerre basis. The use of this orthogonal basis ensures that all of the negative and positive energy states are square integrable, which allows for the application of the standard close-coupling (CC) techniques, and convergence being able to be tested by simply increasing the basis size. It is our belief that any calculations larger than those reported in [1] will not yield substantially different results. It is therefore our hope that the discrepancies between theory and experiment are primarily due to the great difficulties in the experiment associated with working with atomic hydrogen. Nevertheless, a nagging doubt on the validity of theory must remain while there is still discrepancy with experiment for the angular correlation parameters for this simplest electron-atom scattering system.

Even though the CCC method for electron scattering on atomic hydrogen has been unable to resolve the above-mentioned problems, its development has brought considerable success. One way of testing scattering theory is by comparison with model problems. Application of the CCC method to the Poet-Temkin [7,8] model problem of electron-hydrogen scattering, which considers states with only zero orbital angular momentum, and has been solved to a high accuracy, showed that the method yields correct results at all available energies [9]. Furthermore, it demonstrated that the pseudoresonances, which are often associated with square-integrable expansions of the continuum, diminish rapidly and disappear with increasing basis size. We consider these results to be extremely important. This model problem contains most of the difficulties associated with treating exchange as well as the continuum and may be readily used to test the validity of any general scattering theory. To this end we have provided a large set of quantitative results for a number of transitions at an energy range of 1–400 eV for this model problem [10].

Another most important success of the CCC method has been the application to the calculation of the total ionization cross section and spin asymmetry of atomic hydrogen by electron impact [11]. Excellent agreement with experiment indicated that the use of square-integrable representation of the continuum was practical in generating observables involving the true continuum. Once again, due to the large number of states used, no pseu-

*Electronic address: igor@esm.ph.flinders.edu.au

doresonance behavior was evident even though the same set of states was used across a large energy range.

In this work we generalize the CCC method to incorporate hydrogenlike neutral targets Li, Na, and K, as well as ions such as He^+, Li^{2+}, Be^+, and Ar^{7+}, i.e., those targets whose structure is well modeled by the frozen-core Hartree-Fock approximation. We do this for two reasons. The first is that we wish to provide a general and reliable scattering theory that is applicable at all energies and for all transitions, in the hope that it may be useful to others. The second is that we wish to test the method against the many more detailed experiments that are available for these systems in order to perhaps be able to gain some insight as to the problems with atomic hydrogen.

Unfortunately, from the theorist's point of view, comparison of theory with experiment can never validate the theoretical approach, but may certainly invalidate it. The closest a scattering theory can get to being validated is by achieving agreement with a "complete" scattering experiment as envisioned by Bederson [12]. In such experiments all of the quantum observables in a particular transition of interest would be measured, allowing for the most detailed possible check of the calculated scattering amplitudes. Though as yet we are unaware of any such individual experiments, from the point of view of testing theory, it is clear that combining a number of different sets of measurements for various parameters is another way of achieving this goal. Similarly, but more generally, it is our aim to provide a complete scattering theory, i.e., one where all of the individual scattering amplitudes are reliable, irrespective of the projectile energy or transition of interest. In other words, from our point of view, a complete scattering theory is one which is able to provide accurate results not just for a single transition, but all transitions of practical interest at an energy range where the Born approximation is invalid.

The hydrogenlike neutral target for which there exists a large variety of reliable measurements is sodium. In our view, the most important collection of these is that due to McClelland *et al.* [13,14], Scholten *et al.* [15], Kelley *et al.* [16], and Lorentz *et al.* [17]. At an energy range of 1–54.4 eV they measured the ratio of triplet to singlet differential cross sections ($3S$ and $3P$ channels) and also the angular momentum transferred to the atom perpendicular to the scattering plane for both singlet and triplet spin states ($3P$ channel only). Apart from an overall normalization factor, the absolute differential cross section, these measurements are able to test the magnitudes of the spin- and magnetic-sublevel-dependent scattering amplitudes. The resolution of spin is of particular importance to the theorist as the treatment of exchange is one of the more difficult aspects of the calculation. On their own, these measurements have the potential to invalidate many methods of calculation, at least in the projectile energy range considered. We will show that the CCC method for hydrogenlike targets is the only method to date that is not invalidated by these measurements.

It may be considered surprising that the sodium atom would be such a difficult target for theory. As most of the polarization of the atom is due to the $3P$ state it is often believed that scattering should be readily described by a multichannel expansion that treats only the first few discrete states, i.e., higher discrete states as well as the continuum may be readily truncated. Indeed the early 1970s low-energy four-state calculations of Moores and Norcross [18] have not yet been invalidated by experiment to our knowledge. Furthermore, similar calculations above the ionization threshold (see Mitroy, McCarthy, and Stelbovics [19], for example) and perturbative methods such as that of Madison, Bartschat, and McEachran [20] yield quite satisfactory differential cross sections. This is particularly the case for the forward angles, which for the elastic channel are dominated by the polarization of the target due to the $3P$ state. However, application of these methods to the spin resolved data yields quite poor agreement. McCarthy, Mitroy, and Nicholson [21] showed that even a rough treatment of the continuum had a large effect on the results, which generally improved agreement with experiment. A similar observation was made in the work of Madison, Bartschat, and McEachran [20], where the effects of the continuum come in at the second order level. A more accurate treatment of the continuum by Bray [22] also found that its effect was very large and brought about excellent agreement with experiment. Subsequently, we showed [23] that the effect of the continuum came primarily from an allowance for electron flux in the open ionization channels. In a preliminary report of this work [24] we showed that the most accurate treatment of the continuum is provided by the CCC method. It is because the effect of the continuum is so large on even the elastic spin-dependent scattering amplitudes at energies above the ionization threshold, that the treatment of electron-sodium scattering is so difficult.

Much of the CCC theory presented in this work is based on a number of previous publications. The first of these is that of McCarthy and Stelbovics [25], who showed how to formulate and solve the momentum-space coupled Lippmann-Schwinger equations in electron-atom scattering. This partial-wave formalism expanded the projectile using plane waves and so was unsuitable for charged targets. A distorted-wave formalism that was also suitable for charged targets, and generally improved efficiency in the solution of the Lippmann-Schwinger equations, was given by Bray *et al.* [26]. Both of these papers assumed that the potential matrix elements would be complex, due to the inclusion of Q-space states via a polarization (optical) potential. These early applications of the CCO method had rather restrictive approximations for the complex nonlocal polarization potential. A less restrictive form, given by Bray, Konovalov, and McCarthy [27], that utilized symmetric P- and Q-space operators enabled the CCO method to be applicable to the entire range of projectile energies of interest in atomic physics. This method was generalized further by Bray and McCarthy [28] to incorporate a large number of states in P space, as well as showing that the electron–alkali-metal scattering system may be readily treated as a "three-body" problem. The CCC formalism for electron-hydrogen scattering has been given by Bray and Stelbovics [1]. This utilized plane waves for the projectile, but had real potentials. This fact was used to reduce the computational resources necessary to solve the very large

number of coupled integral equations. We combine the ideas of these papers here to present the CCC formalism for hydrogenlike targets that utilizes real potentials and distorted (Coulomb for ions) waves, thus making it applicable to atomic as well as ionic "one-electron" targets.

II. THEORY

We start by assuming that for the purpose of scattering calculations the hydrogenlike target, atom or ion, may be well described by the model of an inert Hartree-Fock core together with a single valence electron. We also allow for an addition of a small phenomenological core polarization potential used to slightly improve the one-electron energies. Under this assumption we first generate the core target states ψ_j by performing a self-consistent-field Hartree-Fock (SCFHF) calculation [29] for the ground state of the target T:

$$\left(K + V^{\rm HF} - \varepsilon_j\right)\psi_j(\boldsymbol{r}) = 0, \qquad \psi_j \in T, \tag{1}$$

where

$$V^{\rm HF}\psi_j(\boldsymbol{r}) = \left(-\frac{Z}{r} + 2\sum_{\psi_{j'}\in T}\int d^3r' \frac{|\,\psi_{j'}(\boldsymbol{r}')\,|^2}{|\,\boldsymbol{r}-\boldsymbol{r}'\,|}\right)\psi_j(\boldsymbol{r}) - \sum_{\psi_{j'}\in T}\int d^3r' \frac{\psi^*_{j'}(\boldsymbol{r}')\psi_j(\boldsymbol{r}')}{|\,\boldsymbol{r}-\boldsymbol{r}'\,|}\psi_{j'}(\boldsymbol{r}). \tag{2}$$

It is worth noting that the core states may also be obtained by performing the SCFHF calculation for the ionic core; see McEachran and Cohen [30], for example. In this way the core states would be optimized for the higher excited states, whereas we have them optimized for the ground state. Since the higher excited states are predominantly hydrogenic they mostly feel the residual charge rather than the core states. For this reason we prefer the optimization for the ground state.

Having defined the core target states $\psi_j \in C$ we can write the frozen-core Hartree-Fock potential $V^{\rm FC}$ as

$$V^{\rm FC}\phi_j(\boldsymbol{r}) = \left(-\frac{Z}{r} + 2\sum_{\psi_{j'}\in C}\int d^3r' \frac{|\,\psi_{j'}(\boldsymbol{r}')\,|^2}{|\,\boldsymbol{r}-\boldsymbol{r}'\,|}\right)\phi_j(\boldsymbol{r}) - \sum_{\psi_{j'}\in C}\int d^3r' \frac{\psi^*_{j'}(\boldsymbol{r}')\phi_j(\boldsymbol{r}')}{|\,\boldsymbol{r}-\boldsymbol{r}'\,|}\psi_{j'}(\boldsymbol{r}), \tag{3}$$

where the notation C indicates the set of frozen core states. The one-electron target Hamiltonian H_2 (index indicates target space) is then given by

$$H_2 = K + V^{\rm FC} + V^{\rm pol}, \tag{4}$$

where we take the often used form for the phenomenological polarization potential (see Zhou *et al.* [31], for example) to be

$$V^{\rm pol}(r) = \frac{-\alpha_d}{2r^4}\left\{1 - \exp\left[-(r/\rho)^6\right]\right\}. \tag{5}$$

Here α_d is the static dipole polarizability of the core and may be obtained for all of the targets of interest to us from McEachran, Stauffer, and Greita [32], for example. The value of ρ is then chosen empirically to fit the one-electron ionization energies.

We are happy to use the form of the polarization potential above only if it has a small effect in the scattering calculation. We do not wish to present a scattering formalism that is significantly affected by phenomenology. Fortunately, we find that most of the interesting effects in the scattering come from the treatment of the dynamics of the interaction rather than that of the structure. The effect of $V^{\rm pol}(r)$ in electron-sodium scattering has been discussed by Bray and McCarthy [28] using the CCO model and has been found to be sufficiently small. For the heavier targets, such as potassium, $V^{\rm pol}(r)$ becomes more important [33] and forms other than (5) may be more suitable. For example, McEachran and Cohen [30] give a nonempirical method for calculating this potential to first order from the core orbitals. It is also worth noting that the above approximations for the structure explicitly exclude real core excitation or ionization, and this places a limitation on the scattering formalism presented. We assume that most of the current measurements are primarily influenced by the interaction of the projectile with the valence electron, though exchange with the core electrons is allowed. This can only be tested by comparison with experiment.

We write the full Hamiltonian of the scattering problem as

$$\begin{aligned} H &= H_1 + H_2 + V_{12} \\ &= K_1 + V_1 + K_2 + V_2 + V_{12}, \end{aligned} \tag{6}$$

where $V_\alpha = V^{\rm FC} + V^{\rm pol}$, with $\alpha = 1, 2$ denoting projectile or target space, respectively. The electron-electron potential is V_{12}. The Schrödinger equation is then

$$(E^{(+)} - H)|\Psi^{S(+)}_{i_0k_0}\rangle = 0, \tag{7}$$

where E is the total energy, $(+) \equiv +i0$ denotes incoming plane- or Coulomb-wave and outgoing spherical-wave boundary conditions, S is the total spin, and i_0, k_0 denote the initial target state and projectile momentum, respectively. The assumption of negligible spin-orbit interaction is implicit in the formalism.

A. Target states

The problem with the standard close-coupling expansions that utilize true discrete and continuum eigenstates is that full inclusion of these states in the close-coupling equations leads to "free-free" V-matrix elements which are computationally too difficult to handle. We avoid this problem by ensuring that at least one of the electrons is represented by a square-integrable function, and so all matrix elements are readily treatable computationally. We allow for one electron to be treated by true continuum functions, unlike in the interaction region of R-matrix methods, and so have no difficulty in the tran-

sition from low to intermediate and high partial waves.

In the CCC formalism we expand $|\Psi_{i_0k_0}^{S(+)}\rangle$ in a set of square-integrable states $|i_n^N\rangle$ which are obtained by performing a diagonalization of the target Hamiltonian (4) in a large truncated Laguerre basis of size N. Thus $|i_n^N\rangle$ satisfy

$$\langle i_m^N|H_2|i_n^N\rangle = \epsilon_n^N \delta_{mn}, \tag{8}$$

where, expanding the notation $|i_n^N\rangle$

$$\langle \boldsymbol{r}|i_n^N\rangle \equiv \langle \boldsymbol{r}|i_{nlm}^{N_l}\rangle = r^{-1}\phi_{nl}^{N_l}(r)Y_{lm}(\hat{\boldsymbol{r}}), \tag{9}$$

we have

$$\phi_{nl}^{N_l}(r) = \sum_{k=1}^{N_l} C_{nk}^l \xi_{kl}(r). \tag{10}$$

The coefficients C_{nk}^l are obtained upon the diagonalization, and the Laguerre basis $\xi_{kl}(r)$ we use is

$$\xi_{kl}(r) = \left(\frac{\lambda_l(k-1)!}{(2l+1+k)!}\right)^{1/2} \times(\lambda_l r)^{l+1}\exp(-\lambda_l r/2)L_{k-1}^{2l+2}(\lambda_l r), \tag{11}$$

where the $L_{k-1}^{2l+2}(\lambda_l r)$ are the associated Laguerre polynomials and k ranges from 1 to the basis size N_l. Thus, for a particular orbital angular momentum l the states $\phi_{nl}^{N_l}(r)$ and corresponding energies $\epsilon_{nl}^{N_l}$ depend on two parameters λ_l and N_l. These parameters may be varied and are typically different for each l. We use N to indicate the full set of states generated for all l in the target state expansion.

The main advantage of the Laguerre basis is that it is orthogonal, unlike the Slater basis, for example, and so we are able to perform the diagonalization with an arbitrarily large N_l without encountering linear dependence problems. This makes our basis ideal for convergence studies. After the diagonalization we have N_l square-integrable states for each l. We order them in ascending values of energy. The negative energy states $\phi_{nl}^{N_l}(r)$ converge pointwise to the true discrete eigenstates $\phi_{nl}(r)$ of the target Hamiltonian as the basis size N_l is increased. Apart from a normalization factor, the positive energy states resemble the true continuum states until the exponential falloff dominates.

In Table I we show the one-electron energies for the four lowest-lying sodium s states arising from the diagonalization of the target Hamiltonian (8) at a range of basis sizes. A difficulty in the CCC method is that since the exponential falloff λ_l in the Laguerre basis is fixed to be the same for each $\phi_{nl}(r)$, $n = 1, N_l$, the generation of the target states is inefficient as a function of basis size. This is indeed evident in Table I, where we see that for $\lambda_s = 2$ a basis size of 30 states is necessary to adequately describe the first four s states. This problem diminishes rapidly with increasing l as the resulting states become more hydrogenic in this case. Fortunately, we often find that convergence in the scattering observable of interest is obtained by using a truncated expansion [24]. By this we mean that even if we obtain say N_l states upon diagonalization, we may use only a subset of these, typically consisting of those states which would lead to open channels. This works very well for the sodium target at the most difficult, intermediate projectile energy range, above the ionization threshold. It may be that we will not be so fortunate for heavier targets. If necessary, we may readily modify the method by replacing the negative energy states with the true eigenstates, and orthogonalize the positive energy states to the eigenstates, together with a suitable modification of the target state energies. This may be helpful for the potassium atom, and ions which have this same isoelectronic sequence.

The full set of N states $|i_n^N\rangle$ form a quadrature rule for the sum and integral over the complete set I of the true target discrete and continuous states $|i\rangle$, i.e.,

$$|\Psi_{i_0k_0}^{S(+)}\rangle = \sum\!\!\!\!\!\!\int_{i\in I} |i\rangle\langle i|\Psi_{i_0k_0}^{S(+)}\rangle = \lim_{N\to\infty}\sum_n |i_n^N\rangle\langle i_n^N|\Psi_{i_0k_0}^{S(+)}\rangle. \tag{12}$$

The nature of the quadrature rule has been discussed in detail by Yamani and Reinhart [34], as well as Stelbovics [35]. This expansion gives rise to the multichannel functions defined by

$$|f_{n0}^{SN}\rangle = \langle i_n^N|\Psi_{i_0k_0}^{S(+)}\rangle, \tag{13}$$

where the zero subscript in $|f_{n0}^{SN}\rangle$ indicates the pair i_0,k_0. For brevity of notation we write

$$|\Psi_{i_0k_0}^{S(+)}\rangle = \lim_{N\to\infty}\sum_n |i_n^N f_{n0}^{SN}\rangle = \lim_{N\to\infty}|\Psi_{i_0k_0}^{SN}\rangle. \tag{14}$$

TABLE I. One-electron energies (eV) of the first four s states of sodium calculated by diagonalizing the target Hamiltonian (8) in a Laguerre basis (11) of varying size N_s and $\lambda_s = 2.0$. The values of α_d and ρ in (5) are 0.99 and 1.44, respectively. See text for more detail. The experimental values are due to Moore [51].

State \ N_s	10	15	20	25	30	Expt.
$3s$	-4.842	-5.077	-5.129	-5.137	-5.139	-5.139
$4s$	-1.881	-1.932	-1.945	-1.946	-1.947	-1.948
$5s$	-0.339	-0.984	-1.019	-1.022	-1.022	-1.024
$6s$	1.828	-1.125	-0.539	-0.614	-0.628	-0.630

B. Coupled equations

In the following we assume that the projectile is an electron, and so exchange must be considered by satisfying antisymmetrization properties of the total wave function. For positron scattering we do not as yet consider positronium formation, and so, by dropping exchange and changing the sign of the relevant potentials, the method is only valid at an energy range where this cross section is negligible. Interestingly, for energies below the Ps formation threshold of atomic hydrogen, convergence in the single-center expansion employed in the CCC formalism is only obtained by inclusion of target states with $l \leq 15$ [36].

Taking the origin to be the center of mass, the total wave function for electron scattering $|\Psi^{S(+)}_{i_0k_0}\rangle$ of the three-body problem satisfies the symmetry property

$$\langle \boldsymbol{r}_1\boldsymbol{r}_2|\Psi^{S(+)}_{i_0k_0}\rangle = (-1)^S\langle \boldsymbol{r}_2\boldsymbol{r}_1|\Psi^{S(+)}_{i_0k_0}\rangle, \tag{15}$$

where $S = 0, 1$ for singlet and triplet scattering, respectively. Thus the multichannel expansion functions (13) are not arbitrary, but satisfy

$$\begin{aligned}\langle i^N_m|f^{SN}_{n0}\rangle &= \langle i^N_m i^N_n|\Psi^{S(+)}_{i_0k_0}\rangle \\ &= (-1)^S\langle i^N_n|f^{SN}_{m0}\rangle.\end{aligned} \tag{16}$$

Using the limit notation a little loosely, the total wave function satisfies the boundary condition

$$\lim_{r_1\to\infty}\langle \boldsymbol{r}_1\boldsymbol{r}_2|\Psi^{S(+)}_{i_0k_0}\rangle = \langle \boldsymbol{r}_1|\boldsymbol{k}^{(+)}_0\rangle\langle \boldsymbol{r}_2|i_0\rangle. \tag{17}$$

To explicitly symmetrize this numerically, we introduce the space exchange operator P_r and write (14) as

$$|\Psi^{S(+)}_{i_0k_0}\rangle = \frac{1}{2}[1 + (-1)^S P_r]\lim_{N\to\infty}|\Psi^{SN}_{i_0k_0}\rangle. \tag{18}$$

The correct boundary conditions are then automatically imposed if we ensure that $|\Psi^{SN}_{i_0k_0}\rangle$ satisfies (17). Note that even without the condition (16) the form (18) satisfies (15). However, such an expansion on its own is too general and leads to nonunique solutions off the energy shell [1].

We are now in a position to derive the coupled equations. Substituting (18) in (7), with $N \to \infty$ limit being implicit, we have

$$\left(E^{(+)} - H\right)|\Psi^{SN}_{i_0k_0}\rangle = (-1)^S\left(H - E^{(+)}\right)P_r|\Psi^{SN}_{i_0k_0}\rangle. \tag{19}$$

Expanding H on the left-hand side, and subtracting an arbitrary distorting potential U_1 from both sides, this becomes

$$\left(E^{(+)} - K_1 - U_1 - H_2\right)|\Psi^{SN}_{i_0k_0}\rangle = V^{SN}_U|\Psi^{SN}_{i_0k_0}\rangle, \tag{20}$$

where

$$\begin{aligned}V^{SN}_U|\Psi^{SN}_{i_0k_0}\rangle &= (V^{SN} - U_1)|\Psi^{SN}_{i_0k_0}\rangle \\ &= \big[V_1 - U_1 + V_{12} \\ &\quad +(-1)^S(H - E^{(+)})P_r\big]|\Psi^{SN}_{i_0k_0}\rangle.\end{aligned} \tag{21}$$

Suitable choices for U_1 will be considered at a later stage.

We now project by $\langle \boldsymbol{k}^{(-)}i^N_n|$, where we use $(-)$ so that $E + i0 - (\epsilon_k - i0) = E + i0 - \epsilon_k$, to get

$$\langle \boldsymbol{k}^{(-)}i^N_n|E^{(+)} - \epsilon_k - \epsilon^N_n|\Psi^{SN}_{i_0k_0}\rangle = \langle \boldsymbol{k}^{(-)}i^N_n|V^{SN}_U|\Psi^{SN}_{i_0k_0}\rangle, \tag{22}$$

and where the use of (8) is implicit, and the distorted-wave states $|\boldsymbol{k}^{(\pm)}\rangle$, discrete and continuous, are solutions of

$$(\epsilon^{(\pm)}_k - K_1 - U_1)|\boldsymbol{k}^{(\pm)}\rangle = 0. \tag{23}$$

In coordinate-space representation

$$\begin{aligned}\langle \boldsymbol{r}|\boldsymbol{k}^{(\pm)}\rangle = (2/\pi)^{1/2}(kr)^{-1}\sum_{L,M} i^L e^{\pm i(\sigma_L+\delta_L)}u_L(k,r) \\ \times Y_{LM}(\hat{\boldsymbol{r}})Y^*_{LM}(\hat{\boldsymbol{k}}),\end{aligned} \tag{24}$$

where σ_L is the Coulomb phase shift, $u_L(k,r)$ is real and has the asymptotic form

$$u_L(k,r) \to F_L(kr)\cos\delta_L + G_L(kr)\sin\delta_L, \tag{25}$$

and $F_L(kr)$ and $G_L(kr)$ are the regular and irregular Coulomb functions, respectively. For plane waves ($U_1 = 0$) both $\sigma_L = 0$ and $\delta_L = 0$. The introduction of the complex phase factor $e^{\pm i(\sigma_L+\delta_L)}$ does not destroy our capacity to solve the coupled equations using primarily real arithmetic.

From (22) we can write

$$\begin{aligned}|\Psi^{SN}_{i_0k_0}\rangle &= |i_0\boldsymbol{k}^{(+)}_0\rangle \\ &\quad + \sum_n \sum\!\!\!\!\!\!\int_{\boldsymbol{k}} \frac{|i^N_n\boldsymbol{k}^{(-)}\rangle\langle \boldsymbol{k}^{(-)}i^N_n|V^{SN}_U|\Psi^{SN}_{i_0k_0}\rangle}{E^{(+)} - \epsilon^N_n - \epsilon_k},\end{aligned} \tag{26}$$

where $|i_0\boldsymbol{k}^{(+)}_0\rangle$ satisfy

$$0 = \left(E^{(+)} - K_1 - U_1 - \epsilon^N_n\right)|i^N_n\boldsymbol{k}^{(+)}_n\rangle \tag{27}$$

$$= \left(E - \epsilon_{k_n} - \epsilon^N_n\right)|i^N_n\boldsymbol{k}^{(+)}_n\rangle, \tag{28}$$

and ensure that the boundary condition (17) is satisfied.

The symmetry condition (16) is implemented by considering the matrix element of V^{SN}_U in (26) which is proportional to E in (21), via

$$\begin{aligned}(-1)^S E\langle \boldsymbol{k}^{(-)}i^N_n|P_r\sum_m|i^N_m f^{SN}_{m0}\rangle \\ = (-1)^S E\sum_m\langle \boldsymbol{k}^{(-)}|i^N_m\rangle\langle i^N_n|f^{SN}_{m0}\rangle \\ = E\sum_m\langle \boldsymbol{k}^{(-)}|i^N_m\rangle\langle i^N_m|f^{SN}_{n0}\rangle \\ = E\langle \boldsymbol{k}^{(-)}i^N_n|I^N_1\sum_m|i^N_m f^{SN}_{m0}\rangle,\end{aligned} \tag{29}$$

where the "identity" operator

$$I_1^N = \sum_n |i_n^N\rangle\langle i_n^N| \tag{30}$$

acts in projectile space. A more general way to implement condition (16) is to introduce an arbitrary nonzero constant θ such that

$$\langle i_n^N|f_{m0}^{SN}\rangle = (1-\theta)\langle i_n^N|f_{m0}^{SN}\rangle + \theta(-1)^S\langle i_m^N|f_{n0}^{SN}\rangle. \tag{31}$$

Then, using (29) and (31) we rewrite (21), dropping the (+) notation, to give

$$\langle \boldsymbol{k}^{(-)} i_n^N|V_U^{SN}|\Psi_{i_0\boldsymbol{k}_0}^{SN}\rangle = \langle \boldsymbol{k}^{(-)} i_n^N|V_1 - U_1 + V_{12} - \theta E I_1^N + (-1)^S[H-(1-\theta)E]P_r|\Psi_{i_0\boldsymbol{k}_0}^{SN}\rangle. \tag{32}$$

We find the interesting result that any nonzero θ in our V_U^{SN} matrix elements leads to a unique solution, and so for simplicity we suppress explicit θ dependence of V_U^{SN}, and take $\theta = 1$. A value of zero still leads to a unique solution on the energy shell, but off the energy shell the results are not unique, which causes numerical instability. For a detailed discussion of these issues see Ref. [37].

Finally, to get a coupled set of Lippmann-Schwinger equations we premultiply (26) by $\langle i_f^N \boldsymbol{k}_f^{(-)}|V_U^{SN}$ and obtain

$$\langle \boldsymbol{k}_f^{(-)} i_f^N|T_U^{SN}|i_0\boldsymbol{k}_0^{(+)}\rangle = \langle \boldsymbol{k}_f^{(-)} i_f^N|V_U^{SN}|i_0\boldsymbol{k}_0^{(+)}\rangle + \sum_n \int\!\!\!\!\!\!\sum_{\boldsymbol{k}} \frac{\langle \boldsymbol{k}_f^{(-)} i_f^N|V_U^{SN}|i_n^N\boldsymbol{k}^{(-)}\rangle\langle \boldsymbol{k}^{(-)} i_n^N|T_U^{SN}|i_0\boldsymbol{k}_0^{(+)}\rangle}{E^{(+)} - \epsilon_n^N - \epsilon_k}, \tag{33}$$

where the T_U^{SN} matrix, for potential $V_U^{SN} = V^{SN} - U_1$, is defined in the usual way

$$\langle \boldsymbol{k}_f^{(-)} i_f^N|T_U^{SN}|i_0\boldsymbol{k}_0^{(+)}\rangle = \langle \boldsymbol{k}_f^{(-)} i_f^N|V_U^{SN}|\Psi_{i_0\boldsymbol{k}_0}^{SN}\rangle. \tag{34}$$

In order to extract physical observables we need to relate the distorted-wave T_U^{SN} matrix to the physical T^{SN} matrix. Following the work of Gell-Mann and Goldberger for eigenstates [38], we rewrite (26) for $U_1 = 0$ as

$$\langle i_f^N|\Psi_{i_0\boldsymbol{k}_0}^{SN}\rangle = |\boldsymbol{k}_f\rangle\delta_{f0} + \frac{1}{E^{(+)} - K_1 - \epsilon_f^N}\langle i_f^N|V^{SN}|\Psi_{i_0\boldsymbol{k}_0}^{SN}\rangle, \tag{35}$$

and using (27) relate the plane waves $|\boldsymbol{k}_f\rangle$ to the distorted waves $|\boldsymbol{k}_f^{(\pm)}\rangle$ by

$$|i_f^N \boldsymbol{k}_f^{(\pm)}\rangle = |i_f^N \boldsymbol{k}_f\rangle + \frac{1}{E^{(\pm)} - K_1 - \epsilon_f^N} U_1 |i_f^N \boldsymbol{k}_f^{(\pm)}\rangle. \tag{36}$$

The physical T^{SN} matrix may then be extracted from the distorted-wave T_U^{SN} matrix by the relation

$$\begin{aligned}\langle \boldsymbol{k}_f i_f^N|T^{SN}|i_0\boldsymbol{k}_0\rangle &\equiv \langle \boldsymbol{k}_f i_f^N|V^{SN}|\Psi_{i_0\boldsymbol{k}_0}^{SN}\rangle \\ &= \langle \boldsymbol{k}_f^{(-)} i_f^N|T_U^{SN}|i_0\boldsymbol{k}_0^{(+)}\rangle \\ &\quad + \langle \boldsymbol{k}_f^{(-)}|U_1|\boldsymbol{k}_0\rangle\delta_{f0}.\end{aligned} \tag{37}$$

We now look at suitable choices for the distorting potential $U_1(r)$. For asymptotically neutral targets we may take $U_1(r) = 0$, i.e., take the plane wave representation of the projectile; see Eq. (23). In this case there are no bound states of the projectile and the sum and integral in (33) becomes simply an integral from zero to infinity over the energies $\epsilon_k = k^2/2$. In performing this integral we wish to ensure that most of the detailed structure in the integrand lies at small ϵ_k. We find that due to the $-Z/r$ factor in (3) the V-matrix elements in (33) go out further with increasing Z, which makes the numerical analysis more difficult. This problem is minimized by taking

$$\begin{aligned}U_1(r) = -\frac{Z}{r} + V^{\rm pol}(r) &+ 2\sum_{\psi_{j'}\in C}\int d^3r' \frac{|\,\psi_{j'}(\boldsymbol{r}')\,|^2}{|\,\boldsymbol{r}-\boldsymbol{r}'\,|} \\ &+ \int d^3r' \frac{|\phi_j(\boldsymbol{r}')|^2}{|\,\boldsymbol{r}-\boldsymbol{r}'\,|},\end{aligned} \tag{38}$$

where we typically take ϕ_j to be the ground state. This form of the potential removes the $-Z/r$ factor in (32) due to V_1 and so ensures shortest-ranged V-matrix elements. For neutral targets this potential is asymptotically zero, but for charged targets it is the Coulomb potential due to the residual charge. Therefore, the required boundary conditions are satisfied by this form of the potential for both neutral and charged targets. This form of the distorting potential usually leads to a number of bound states, in fact an infinite set in the case of ionic targets. We include as many of these as necessary for convergence in (33), typically around five per partial wave.

Note that apart from the asymptotic part, the choice of the potential in the inner region is arbitrary. The results for T^{SN} must be independent of the choice of $U_1(r)$ for small r, which we check by varying ϕ_j in (38). The choice above is purely a numerical technique in order to simplify the solution of the integral equations (33).

C. Solving the coupled Lippmann-Schwinger equations

We solve the coupled Lippmann-Schwinger equations for the distorted-wave T matrix by expanding (33) in partial waves J of the total orbital angular momentum. The reduced V (or T) matrix elements are defined by

$$\langle Lk^{(-)}ln \mid\mid V_{J\Pi}^{SN} \mid\mid n'l'k'^{(+)}L' \rangle = \sum_{\substack{M,m \\ M',m'}} C_{LlJ}^{MmM_J} C_{L'l'J}^{M'm'M_J} \int d\hat{\boldsymbol{k}} \int d\hat{\boldsymbol{k}}' Y_{LM}^*(\hat{\boldsymbol{k}}) Y_{L'M'}(\hat{\boldsymbol{k}}') \langle \boldsymbol{k}^{(-)} i_{nlm}^{N_l} \mid V_U^{SN} \mid i_{n'l'm'}^{N_{l'}} \boldsymbol{k}'^{(+)} \rangle, \tag{39}$$

where $\Pi = (-1)^{l+L} = (-1)^{l'+L'}$ is parity and C denotes a Clebsch-Gordan coefficient. For scattering on a nS state we require matrix elements corresponding only to the "natural" parity $\Pi = (-1)^J$. If scattering on target states with nonzero orbital angular momentum then the separate set of equations corresponding to the "unnatural" parity $\Pi = (-1)^{J+1}$ also arises. The reduced matrix elements may be evaluated with the use of Eqs. (9), (24), and (32).

All radial integrals are calculated to a specified accuracy, typically 0.01%, which is varied to ensure stability of the results. This is achieved by integrating out to around 200 or 300 a.u. on a sufficiently fine radial mesh. Variation of the cutoff radius and the spacing in the radial mesh is used to control the precision of the calculation. For the most long-ranged integrals, which fall off as $1/r^2$, we can also complete the integration to $r = \infty$ by employing analytical techniques, though this is rarely necessary.

We now proceed in the same way as in Ref. [1], which we incorporate here for completeness and ease of reference. In order to reduce the problem of solving the coupled equations using primarily real arithmetic we define the K matrix in terms of the T matrix by

$$\begin{aligned} \langle Lk_{nl}ln \mid\mid K_{J\Pi}^{SN} \mid\mid n_0l_0k_0L_0 \rangle = & \sum_{l',L'} \sum_{n'=1}^{N_{l'}^o} \langle Lk_{nl}ln \mid\mid T_{J\Pi}^{SN} \mid\mid n'l'k_{n'l'}L' \rangle \\ & \times \left(\delta_{l'l_0} \delta_{L'L_0} \delta_{n'n_0} + i\pi k_{n'l'} \langle L'k_{n'l'}l'n' \mid\mid K_{J\Pi}^{SN} \mid\mid n_0l_0k_0L_0 \rangle \right), \end{aligned} \tag{40}$$

where k_{nl} is defined for $1 \le n \le N_l^o \le N_l$ for which

$$k_{nl} = \sqrt{2(E - \epsilon_{nl})} \tag{41}$$

is real. In this case we say that the channel nlL is open, and if $E < \epsilon_{nl}$ we say that this channel is closed. For a particular l the number of states which lead to open channels is N_l^o.

With this definition, substitution into the partial-wave expansion of (33) results in

$$\begin{aligned} \langle Lk_{nl}ln \mid\mid K_{J\Pi}^{SN} \mid\mid n_0l_0k_0L_0 \rangle = & \langle Lk_{nl}ln \mid\mid V_{J\Pi}^{SN} \mid\mid n_0l_0k_0L_0 \rangle \\ & + \sum_{l',L'} \sum_{n'=1}^{N_{l'}} \mathcal{P} \sum\!\!\!\!\!\!\int_{k'} \frac{\langle Lk_{nl}ln \mid\mid V_{J\Pi}^{SN} \mid\mid n'l'k'L' \rangle}{E - \epsilon_{n'l'} - \epsilon_{k'}} \langle L'k'l'n' \mid\mid K_{J\Pi}^{SN} \mid\mid n_0l_0k_0L_0 \rangle. \end{aligned} \tag{42}$$

This is solved for the K matrix using real arithmetic, and the T matrix is obtained by solving the much smaller set of equations (40). Note that the K and V matrices are actually complex due to the phase factors in (24), but as these factors occur as complex conjugates in the integrand above, they are trivially factored out. The notation $\mathcal{P}$ is used to denote a principle-value-type integral for $k' \in [0, \infty)$ with corresponding energy in the denominator $\epsilon_{k'} = k'^2/2$. The introduction of the potential U_1 requires the summation over all of the bound states ($\epsilon_{k'} < 0$) of this potential. Note that the sum over n' in (42) may be truncated to include fewer states than those generated by the Laguerre basis size $N_{l'}$. For energies above the ionization threshold, we typically obtain convergence by truncating this sum at $N_{l'}^o$, i.e., use only those states which generate open channels.

We solve the coupled integral equations (42) for each partial wave J, parity Π, and total spin S by replacing the integral with a quadrature rule. The bound states then become like extra quadrature points with unity for the weight function. There are many possible choices for quadrature rules; see Bransden, Noble, and Hewitt [39] and references therein, for example. There does not appear to be one choice that is superior to all others, and so a little flexibility is required. The major problem to overcome is that due to the singularity whose position is dependent on the intermediate energy $E - \epsilon_{n'l'}$. We address this by splitting the integral into a number of intervals, one of which is symmetric about the singularity. We treat the singularity by taking an even number of Gaussian points in this interval. Convergence, with respect to the integration over k' in (42), is established by variation in the number of points in each interval; see [1] for a little more detail.

On replacement of the integral by a quadrature rule, (42) may be written in shortened notation as

$$K_{fi}^{SN} = V_{fi}^{SN} + \sum_n w_n V_{fn}^{SN} K_{ni}^{SN}, \tag{43}$$

where the single sum over n contains all of the sums in (42). The weights w_n contain the integration weights divided by the energy term. To solve this equation we form a closed set of linear equations by letting f run over the same range as n. Replacing f by n' to indicate this, we have

$$V^{SN}_{n'i} = \sum_n \left(\delta_{n'n} - w_n V^{SJ}_{n'n}\right) K^{SN}_{ni}$$
$$= \sum_n \left(\delta_{n'n}/w_n - V^{SN}_{n'n}\right) w_n K^{SN}_{ni}. \quad (44)$$

As both $\delta_{n'n}/w_n$ and $V^{SN}_{n'n}$ are symmetric on interchange of n and n' we need to solve the linear system of the form $AX = B$, where A is a real symmetric matrix.

In the earlier work [1] this was done by storing the matrix A in compact (one-dimensional) form. However, this requires further computational storage, on top of the V matrix elements. Here we avoid extra storage for A by using V for both storing the potential matrix elements and in solving the resultant linear equations. To do this we store the singlet ($S = 0$) $V^{SN}_{n'n}$ matrix elements in the top half of $A_{n'n}$ and the triplet ($S = 1$) elements in the bottom half, taking care that both the singlet and triplet diagonals are stored correctly. Invoking the LAPACK routine SSYSV [40] first for the singlet case solves the linear symmetric system $AX = B$ without destroying the bottom half of A, which contains the triplet potential matrix elements. A subsequent call to SSYSV solves the triplet linear equations. The size of the calculation is then dependent primarily on the storage required for the V-matrix elements. For example, a typical large calculation that treats 100 channels with 50 quadrature points in each results in a 5000×5000 single-precision real matrix which takes 100M of core memory storage. On our SUN SS10/512 two-processor workstation with 256M of memory we may readily run two such large calculations simultaneously.

We find this nonperturbative method to be the most efficient way of solving the linear equations for the lower partial waves. However, we can also employ an iterative procedure such as given by Schneider and Collins [41], which is guaranteed to converge, and does so rapidly for the higher partial waves.

The number of partial waves J for which (42) is solved varies as a function of energy. In the calculations considered we progressively increase from maximum $J = 10$ at 1.0 eV to $J = 80$ at 54.4 eV. Upon solution of (42) for the K matrix, the T-matrix elements are found by solving (40) which are then used directly to generate the scattering amplitudes. There are no averaging procedures of any kind.

III. RESULTS

In this section we test the CCC method for electron scattering on hydrogenlike targets by application to electron-sodium scattering. It is for this electron-hydrogenlike target scattering system that there exists arguably the most wide range of detailed experimental data. The existence of spin resolved measurements at a range of projectile energies of 1–54 eV allows for an unprecedented test of the theoretical approaches. We apply the CCC theory at every energy where these data are available, as well as at a few other energies where there is some other detailed experimental data.

A. Some definitions

From the partial T-matrix elements of (40) we generate the magnetic-sublevel and spin-dependent scattering amplitudes $f^S_{m_f m_i}(\theta)$ in the collision frame (z axis is parallel to the projectile) for the transition $n_i l_i$ to $n_f l_f$, where $-l_i \le m_i \le l_i$ and $-l_f \le m_f \le l_f$. These have the symmetry properties

$$f^S_{m_f m_i}(\theta) = (-1)^{m_f - m_i} f^S_{-m_f - m_i}(\theta). \quad (45)$$

For scattering from s states it is convenient to drop all reference to the pair $l_i m_i$ and drop the index on m_f, which we will do as in this work we are interested in scattering from the ground state of sodium.

For elastic scattering we also drop reference to the pair $l_f m_f$ and write the differential cross section as

$$\sigma_{3s}(\theta) = [|f^0(\theta)|^2 + 3|f^1(\theta)|^2]/4. \quad (46)$$

The ratio of triplet to singlet scattering is given by

$$r_{3s}(\theta) = |f^1(\theta)|^2/|f^0(\theta)|^2, \quad (47)$$

which is related to the (up-down) spin asymmetry

$$A_{3s}(\theta) = \frac{1 - r_{3s}(\theta)}{1 + 3r_{3s}(\theta)}. \quad (48)$$

For the purpose of presentation of results we prefer the use of the spin asymmetry rather than the ratio as the former always stays finite, ranging between $-1/3$ when triplet scattering is dominant ($r = \infty$) and $+1$ when singlet scattering is dominant ($r = 0$). An additional determination of the phase between the singlet and triplet scattering amplitudes would complete the determination of observables for elastic scattering.

For excitation of the $3P$ state the characterization of the scattering is more complicated and has attracted a considerable amount of attention. For a comprehensive review of the subject see Anderson, Gallagher, and Hertel [42]. Here the charge cloud is conveniently described in the more physical so-called natural frame, where the z axis is perpendicular to the scattering plane. The collision-frame amplitudes may be transformed to this frame by

$${}^n f^S_{\pm 1}(\theta) = \mp f^S_0(\theta)/\sqrt{2} - i f^S_1(\theta). \quad (49)$$

A set of seven independent parameters that are sufficient to complete the determination of this scattering process have been proposed by Anderson and Bartschat [43]. However, for the purpose of testing theory with experiment, it is most convenient to compare the theoretical results with data that are as close as possible to the direct measurements. This is particularly so when there is a variety of complimentary data, but which are at different projectile energies, a point noted in [43].

For the transition between the $3S$ and $3P$ states of sodium we may define the spin-dependent differential cross section by

$$\sigma^S_{3p}(\theta) = |f^S_0(\theta)|^2 + 2|f^S_1(\theta)|^2. \quad (50)$$

The spin-averaged differential cross section, ratio of triplet to singlet scattering, and the equivalent spin asymmetry are respectively given by

$$\sigma_{3p}(\theta) = [\sigma^0_{3p}(\theta) + 3\sigma^1_{3p}(\theta)]/4, \quad r_{3p}(\theta) = \sigma^1_{3p}(\theta)/\sigma^0_{3p}(\theta), \tag{51}$$
$$A_{3p}(\theta) = [\sigma^0_{3p}(\theta) - \sigma^1_{3p}(\theta)]/\sigma_{3p}(\theta).$$

We now define the spin-dependent angular correlation parameters $[\lambda^S(\theta), R^S(\theta), I^S(\theta)]$ in terms of reduced Stokes parameters $P^S_k(\theta)$, $k = 1, 2, 3$, which may be combined to give the spin-averaged parameters using the relation

$$P_k(\theta) = \frac{P^0_k(\theta) + 3r_{3p}(\theta)P^1_k(\theta)}{1 + 3r_{3p}(\theta)}, \tag{52}$$

where

$$\begin{aligned} P^S_1(\theta) &= [|f^S_0(\theta)|^2 - 2|f^S_1(\theta)|^2]/\sigma^S_{3p}(\theta) \\ &= -2\,\mathrm{Re}[{}^n f^S_1(\theta)\,{}^n f^{S*}_{-1}(\theta)]/\sigma^S_{3p}(\theta) \\ &= 2\lambda^S(\theta) - 1, \end{aligned} \tag{53}$$

$$\begin{aligned} P^S_2(\theta) &= -2\sqrt{2}\,\mathrm{Re}[f^S_1(\theta)f^{S*}_0(\theta)]/\sigma^S_{3p}(\theta) \\ &= 2\,\mathrm{Im}[{}^n f^S_1(\theta)\,{}^n f^{S*}_{-1}(\theta)]/\sigma^S_{3p}(\theta) \\ &= -2\sqrt{2}R^S(\theta), \end{aligned} \tag{54}$$

$$\begin{aligned} P^S_3(\theta) &= 2\sqrt{2}\,\mathrm{Im}[f^S_1(\theta)f^{S*}_0(\theta)]/\sigma^S_{3p}(\theta) \\ &= [|{}^n f^S_{-1}(\theta)|^2 - |{}^n f^S_1(\theta)|^2]/\sigma^S_{3p}(\theta) \\ &= 2\sqrt{2}I^S(\theta). \end{aligned} \tag{55}$$

Having defined these parameters explicitly in terms of the scattering amplitudes we relate these to the physical charge cloud orientation, alignment, and total coherence parameters [42] by

$$\begin{aligned} &L_\perp(\theta) = -P_3(\theta), \quad P_l(\theta)\exp[2i\gamma(\theta)] = P_1(\theta) + iP_2(\theta), \\ &P^+(\theta) = \sqrt{P_1(\theta)^2 + P_2(\theta)^2 + P_3(\theta)^2}. \end{aligned} \tag{56}$$

Finally, we give the relation for the (left-right) spin asymmetry function S_A measured by Nickich *et al.* [44] as

$$S_A(\theta) = \frac{L^0_\perp(\theta) - r_{3p}(\theta)L^1_\perp(\theta)}{1 + 3r_{3p}(\theta)}. \tag{57}$$

We do not wish to discuss the physical significance of the parameters defined above. This has been adequately covered in the literature, in particular in Ref. [42]. We present their definitions here for completeness and ease of reference.

B. Comparison with experiment

It must be remembered that we treat electron scattering on sodium by the model of two electrons and a frozen Hartree-Fock core. Though we allow for core exchange and virtual excitation of the core by means of a small phenomenological polarization potential, we have no allowance for real core excitation or ionization. We therefore cannot necessarily expect *a priori* complete quantitative agreement with experiment. This is unfortunate because if we do find discrepancy with experiment it may be difficult to establish whether the problem is due to theory or experiment. Having said this, the excellent agreement with various measurements we find below indicates that this model of treating electron scattering on sodium as a three-body problem is very good.

The utility of the CCC formalism is only achieved provided that convergence in the observables of interest is obtained as a function of ever increasing number of states in the multichannel expansion. By convergence we mean that any larger calculation would not alter the presented results significantly. The rate of convergence depends on the observable and projectile energy. Detailed angular measurements typically require more states for accuracy at each angle than say the integrated result. At low and high energies convergence is more rapid and is often obtained by expansion in just the first few discrete states. It is for this reason that in the calculations presented below there is a large variation in the basis sizes and number of states used. For example, at the lower projectile energies we take rather large basis sizes in order to generate more open channels. In these cases calculations are relatively insensitive to the exponential falloff parameter λ_l. This is due to the fact that with large basis sizes the true low-lying discrete eigenstates are readily reproduced; see Table I. However, at higher energies we use smaller basis sizes so as to limit the number of open channels to a number that may be readily handled with our computational facilities. In these cases the values of λ_l are more carefully chosen so as to reproduce the ground and first few excited eigenstates. Interestingly, we find that except at the very low and very high energies, convergent results are obtained coupling roughly the same number of states. At all of the projectile energies presented below we have performed many calculations with varying basis sizes N_l, number of states used within a particular basis, λ_l, and maximum $l \leq 3$. At most energies in excess of ten calculations were performed checking convergence. For simplicity of presentation in the figures below we present only the largest of these at each projectile energy. We believe that any calculation larger than those presented will not yield significantly different results.

We begin by looking at projectile energies of 1, 1.6, and 54.4 eV in Fig. 1. At these energies there exist very accurate measurements of the elastic spin asymmetry [Eq. (48)] summarized in Kelley *et al.* [16] as well as spin-averaged $L_\perp$ [Eqs. (52), (55), and (56)] at the largest energy by McClelland, Kelley, and Celotta [13]. We combined these together in order to show that very large calculations that treat the same number of states can be applied at both low and high energies. At the very low energies excellent agreement with experiment is achieved by only including the first few (typically $3S, 3P, 4S$) discrete states in the close-coupling formalism. It is a very important test of the method that it yield the same result with a very much larger set of states. It may seem trivial that this should be the case. A careful investigation of the term containing I^N_1 in (32) shows that as the number of states is increased all of the diagonal V-matrix

elements change. The larger basis sizes also introduce greater complexity to the V-matrix elements requiring a much larger quadrature mesh in order to solve the linear equations accurately. The subsequent solutions of the linear equations must and do yield the same single elastic result.

The calculation denoted by CCC was generated by taking the lowest in energy (excluding core) $12s$ ($N_s = 20, \lambda_s = 2.6$), $11p$ ($N_p = 14, \lambda_p = 1.8$), $10d$ ($N_d = 12, \lambda_d = 1.5$), and $9f$ ($N_f = 10, \lambda_f = 1.5$) states. The reason some of the higher-energy states were omitted is that at 54.4 eV they lead to closed channels. In particular, at 54.4 eV the sum over n' in both (40) and (42) ranges up to N_l^o, where $N_s^o = 12$, $N_p^o = 11$, $N_d^o = 10$, and $N_f^o = 9$. At 1.0 and 1.6 eV we used the same values in (42), but in (40) only $N_s^o = 1$ is nonzero. For all of the observables considered in this work, at projectile energies above the ionization threshold, we find that convergence is obtained in the use of just open channels. This confirms our earlier finding [23] that the effect of the continuum on the scattering phenomena between the lowest-lying states comes in primarily due to allowance of flux in the ionization channels. For comparison we also present the results of our CCO and CC methods [28]. The latter treats the first 15 discrete eigenstates, which are sufficient to obtain convergence in just the discrete spectrum. The former also adds the effect of the continuum via a complex nonlocal polarization (optical) potential generated from true continuum states, but subject to approximation. Comparison of the CC calculation with either the CCC or CCO directly indicates the effect of the continuum. Though the CCC method treats the continuum more accurately, the size of our computational facilities do not allow us to have simultaneously large basis sizes N_l and many l. In all of the CCC calculations below we have $l \leq 3$, whereas the CCO method has $l \leq 5$. We typically find that the CCC and CCO results are very similar, with CCC being in better agreement with experiment, indicating that it is more important to treat smaller l accurately than $l > 3$. All three calculations give a good reproduction of the experiment in Fig. 1, with CCC being the best for the elastic spin asymmetry at 54.4 eV. It is worthwhile noting the remarkable agreement with the $L_\perp$ parameter. This is directly related to angular correlation parameter I, see Eq. (55), with which agreement at this energy in atomic hydrogen is considerably worse [1].

In Fig. 2 we look at a single projectile energy of 4.1 eV. Here we have both the elastic $3S$ and inelastic $3P$ channels open. The measurements of spin asymmetries [Eqs. (48) and (51)] and spin-resolved $L_\perp^S$ [Eqs. (55) and (56)] may be found in Kelley *et al.* [16]. We see that there is little difference between the CCC, CCO, and CC theories, which are in good agreement with experiment. The CCC calculation used $13s$ ($N_s = 30, \lambda_s = 2.6$), $12p$

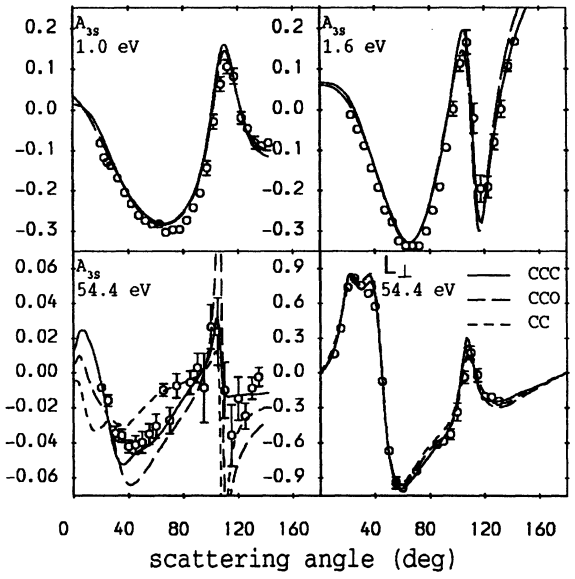

FIG. 1. Elastic spin asymmetries A_{3S} at 1.0, 1.6, and 54.4 eV, as well as $L_\perp$ at 54.4 eV, for electron scattering on the ground state of sodium. The convergent close-coupling (CCC) calculation couples $12s$, $11p$, $10d$, and $9f$ Laguerre basis states (see text for detail). The coupled-channel optical (CCO) method [28] couples the first 15 ($3 \leq n \leq 6$ and $0 \leq l \leq 3$) discrete eigenstates, with the effect of continuum states with $l \leq 5$ included via a complex polarization potential. The CC calculation denotes a standard close-coupling calculation that truncates the multichannel expansion after convergence in the use of just the discrete target eigenstates has been obtained. These are the same 15 states used in the CCO calculation [28]. The measurements are due to McClelland, Kelley, and Celotta [13] and Kelley *et al.* [16], with the error bars only shown if they are larger than the size of the symbol denoting the experiment. Quantitative results may be obtained by correspondence with the author.

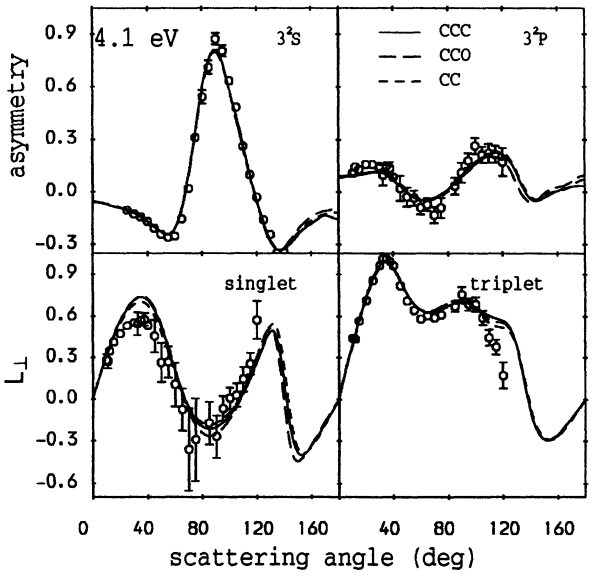

FIG. 2. Elastic A_{3S} and inelastic A_{3P} spin asymmetry, singlet and triplet $L_\perp$ for electron scattering on sodium at 4.1 eV. The CCC calculation couples $13s$, $12p$, $11d$, and $6f$ Laguerre basis states (see text for detail). The CCO and CC theories, as well as experiment, are as in Fig. 1.

($N_p = 29, \lambda_p = 1.8$), $11d$ ($N_d = 28, \lambda_d = 1.5$), and $6f$ ($N_f = 27, \lambda_f = 1.5$) states. Note that the basis sizes are very large, which was done in order to make sure that all of the above states lead to open channels. The discrepancy with experiment around 40° with the singlet $L_\perp$ and around 120° with the triplet $L_\perp$ is a little disappointing. The same features are also found in the 11 state R-matrix calculations of Zhou, Norcross, and Whitten [45]. As mentioned earlier, for targets whose structure is treated subject to approximation, it is very difficult to state with any confidence as to the source of discrepancy with experiment. Generally, we find agreement at this energy is very good, and we will see that at other energies agreement with experiment is even better.

The results at a projectile energy of 10 eV are presented in Fig. 3. Here we see that the CC calculation is at times significantly different from both the CCC and CCO, indicating that continuum is important. For the singlet $L_\perp$ we see that it is only the CCC theory that is able to reproduce the experiment. In fact we have remarked in our earlier CCO work [28] that this parameter may serve as a test case of accurate treatment of the effects of the continuum. It is particularly pleasing that this has proved to be the case. The CCC calculation couples $14s$ ($N_s = 30, \lambda_s = 2.0$), $13p$ ($N_p = 29, \lambda_p = 2.0$), $12d$ ($N_d = 20, \lambda_d = 1.5$), and $8f$ ($N_f = 14, \lambda_f = 1.5$) states. All except the last two s, p, d, and one f states lead to open channels. We added the seven extra states in order to verify that they have little effect. Until the advent of CCC for sodium it was the CCO theory which best described the observables of interest here. Comparison with the second-order calculations of Madison, Bartschat, and McEachran [20] may be found in our earlier work. It is interesting to note that by contrast to the singlet $L_\perp$, the triplet $L_\perp$ is readily described by just the CC theory. In fact, we generally find that the singlet observables are more sensitive to the details of the theory than triplet ones. It is difficult to specify why this may be the case, perhaps, as suggested to us by Norcross, it is due to a greater electron-electron correlation in singlet states. The lack of sensitivity of the triplet observables, as well as their statistical weight being three times that of the singlet [see Eq. (52)], may explain why more approximate methods of calculation often do much better for the spin-averaged observables than for the singlet ones [20].

The energy where the effects of the continuum are most evident is that of 20 eV. The results are presented in Fig. 4. Both the elastic and inelastic spin asymmetries are not even qualitatively described by the CC theory, which is convergent in the use of just the discrete eigenstates. The similarity of the CCO and CCC calculations indicates convergence in the CCC calculation which was obtained by coupling $13s$ ($N_s = 20, \lambda_s = 2.4$), $12p$ ($N_p = 17, \lambda_p = 2.0$), $9d$ ($N_d = 13, \lambda_d = 1.7$), and $8f$ ($N_f = 12, \lambda_f = 1.5$) states. Note that we are decreasing the basis sizes with increasing projectile energy so as to limit the number of open channels. As at 10 eV, to check our hypothesis that only open channels are necessary above the ionization threshold six of the highest energy states included in the calculation resulted in closed channels. Again we found that they have minimal effect, and we only present the results of the largest calculation performed. By looking at the larger angles we see that the CCC method is in better agreement with experiment than the CCO results, indicating once more the importance of treating the lower target partial waves

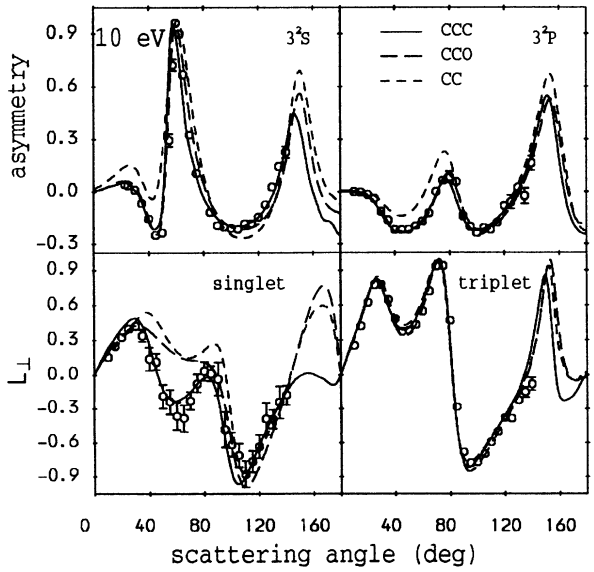

FIG. 3. Elastic A_{3S} and inelastic A_{3P} spin asymmetry, singlet and triplet $L_\perp$ for electron scattering on sodium at 10 eV. The CCC results have been generated using $14s$, $13p$, $12d$, and $8f$ Laguerre basis states (see text for detail). The CCO and CC theories, as well as experiment, are as in Fig. 1.

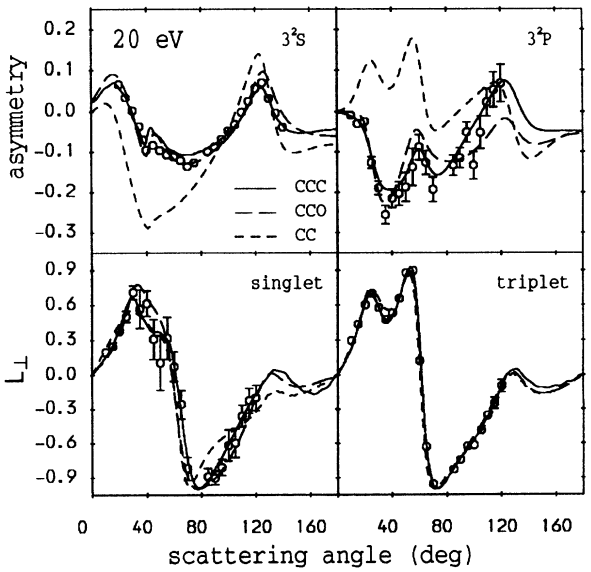

FIG. 4. Elastic A_{3S} and inelastic A_{3P} spin asymmetry, singlet and triplet $L_\perp$ for electron scattering on sodium at 20 eV. The CCC results have been generated using $13s$, $12p$, $9d$, and $8f$ Laguerre basis states (see text for detail). The CCO and CC theories, as well as experiment, are as in Fig. 1.

more accurately than treating the higher partial waves.

This is also evident at 40 eV shown in Fig. 5. Here all three theories adequately describe both of the $L_\perp$ parameters, but it is the CCC theory which yields best agreement with the inelastic spin asymmetries. These results were generated with $9s$ ($N_s = 16, \lambda_s = 2.6$), $10p$ ($N_p = 15, \lambda_p = 2.0$), $9d$ ($N_d = 11, \lambda_d = 1.5$), and $6f$ ($N_f = 8, \lambda_f = 1.0$) states, all of which generate open channels.

It is also interesting to note the behavior of some of these parameters as a function of projectile energy. For example, we can look at the elastic spin asymmetry at projectile energies of 1, 1.6, 4.1, 10, 20, 40, and 54.4 eV and observe the variation in the structure. In doing this we see how the peak that starts at around 120° moves to smaller angles, then rapidly diminishes between 10 and 20 eV, so that it is only just visible at 20 eV, and then becomes a trough.

This completes the application of the CCC theory to the spin-resolved data from Refs. [13–17]. We now look at spin-averaged reduced Stokes parameters [Eqs. (52)–(55)] measured by Scholten, Shen, and Teubner [46] and Sang *et al.* [47]. The comparison of the measurements and the CC, CCO, and CCC theories at projectile energy of 12.1 eV is presented in Fig. 6. For interest we also relate the measurements to the physical orientation, alignment, and coherence parameters, as discussed in Sec. III A [Eq. (56)]. The CCC results were generated using $13s$ ($N_s = 30, \lambda_s = 2.0$), $12p$ ($N_p = 26, \lambda_p = 1.8$), $12d$ ($N_d = 23, \lambda_d = 1.5$), and $8f$ ($N_f = 15, \lambda_f = 1.5$) states, all of which generate open channels. We see that there is very little to separate the theories. All three can be said to be in excellent agreement with both sets of measurements. However, a more detailed observation shows that given the very small error bars in the two sets of measurements, the theory favors the measurements of Scholten, Shen, and Teubner.

A similar situation occurs at 22.1 eV, presented in Fig. 7, where the CCC results were generated using $12s$ ($N_s = 24, \lambda_s = 2.4$), $12p$ ($N_p = 21, \lambda_p = 2.0$), $11d$ ($N_d = 18, \lambda_d = 2.0$), and $9f$ ($N_f = 12, \lambda_f = 1.5$) states, all of which lead to open channels. Once again there is not much difference between the theories, though it is clear that the CCO and CCC theories are better. The small error bars of the two sets of measurements of the Stokes parameters allows us to differentiate between the two experiments. What is remarkable is the apparent sensitivity of the derived parameters, particularly P_l and P^+. These differentiate between the two experiments much more so than the Stokes parameters. Similarly, the dip around 60° for the P^+ parameter is considerably lower in the experiment than theory due to the very small

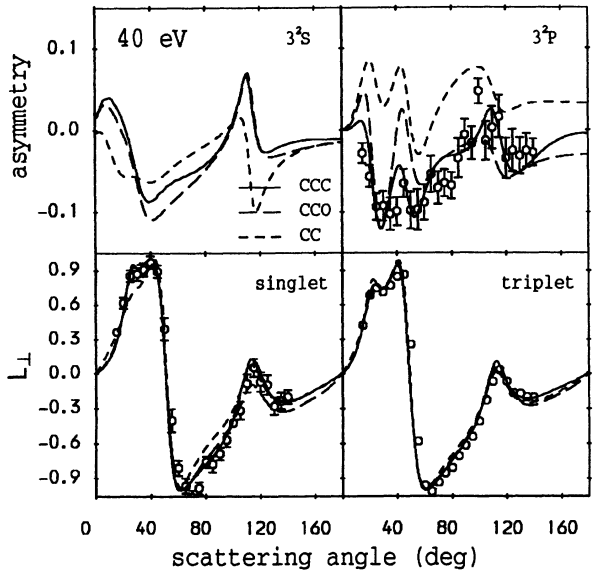

FIG. 5. Elastic A_{3S} and inelastic A_{3P} spin asymmetry, singlet and triplet $L_\perp$ for electron scattering on sodium at 40 eV. The CCC results have been generated using $9s$, $10p$, $9d$, and $6f$ Laguerre basis states (see text for detail). The CCO and CC theories, as well as experiment, are as in Fig. 1.

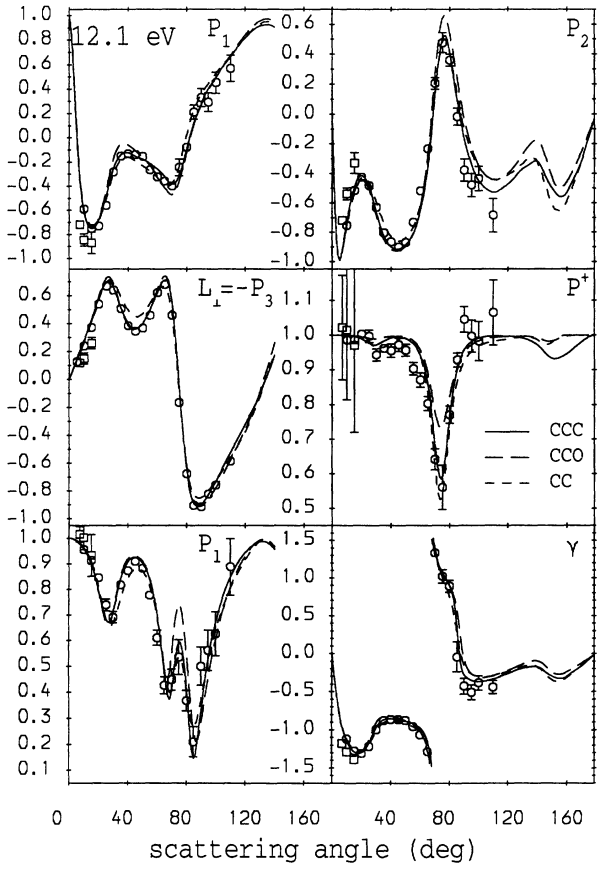

FIG. 6. $3\,^2P$ reduced Stokes parameters P_1, P_2, and P_3, and derived orientation, alignment, and coherence parameters $L_\perp$, P_l, γ, and P^+ at projectile energy of 12.1 eV incident on the ground state of sodium. The CCC results have been generated using $13s$, $12p$, $12d$, and $8f$ Laguerre basis states (see text for detail). The CCO and CC theories are as in Fig. 1. The measurements due to Scholten, Shen, and Teubner [46], and Sang *et al.* [47] are denoted by ○ and □, respectively. Error bars shown only if larger than the symbol denoting the experiment.

discrepancy with the measured P_2 parameter at 55° and 60°. Given the very large rate of change in P_2 at these angles we are not perturbed by the apparent discrepancy with experiment.

Though the measurements of the spin-averaged reduced Stokes parameters provides for a good test of theory, we see that they do not provide as strong a test of theory as do measurements using spin-polarized projectiles and targets. Since the reduced Stokes parameters are directly related to the angular correlation parameters λ and R [Eqs. (53) and (54)] with which there is discrepancy in atomic hydrogen, good agreement in electron scattering on sodium we find very encouraging.

A set of measurements which used a spin-polarized electron incident on an unpolarized sodium atom has been provided by Nickich *et al.* [44] in the form of the (left-right) spin asymmetry function S_A; see Eq. (57). We compare our results with their measurements at 8.1, 10, 12.1, and 22.1 eV incident projectile energy in Fig. 8. The CCC results were generated using the scattering amplitudes from calculations described above at corresponding projectile energies. At the lowest energy we used

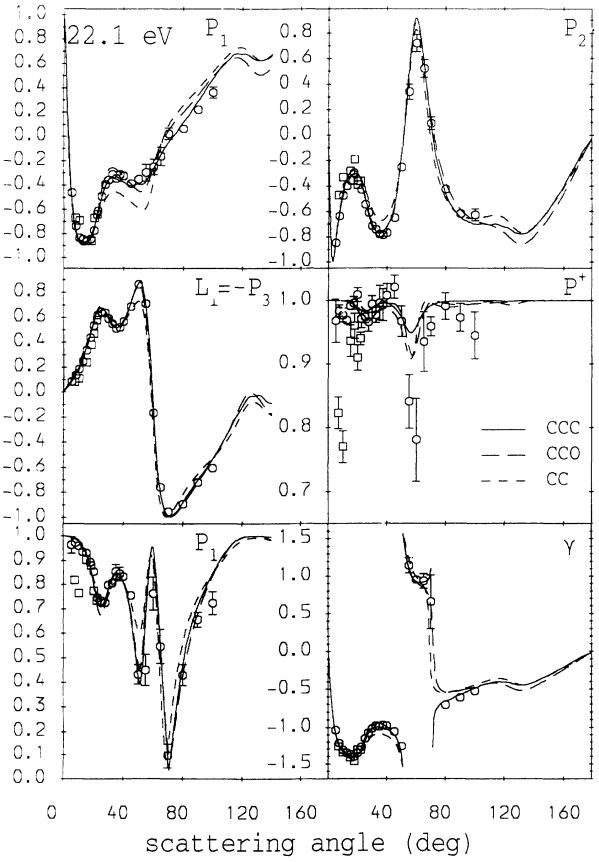

FIG. 7. $3\,^2P$ reduced Stokes parameters P_1, P_2, and P_3, and derived orientation, alignment, and coherence parameters $L_\perp$, P_l, γ, and P^+ at projectile energy of 22.1 eV incident on the ground state of sodium. The CCC results have been generated using $12s$, $12p$, $11d$, and $9f$ Laguerre basis states (see text for detail). The CCO and CC theories are as in Fig. 1. The measurements are as in Fig. 6.

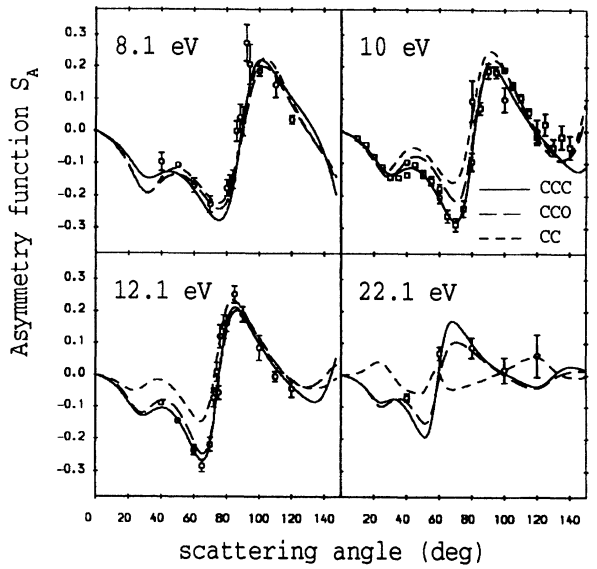

FIG. 8. $3\,^2P_{1/2}$ left-right spin asymmetry function S_A at projectile energies of 8.1, 10, 12.1, and 22.1 eV incident on the ground state of sodium. At 8.1 eV the CCC results have been generated using the same set of states as at 10 eV (see text for detail). At other energies the same sets as specified in Figs. 3, 6, and 7 were used. The CCO and CC theories are as in Fig. 1. The measurements denoted by ○ and □ are due to Nickich *et al.* [44] and Kelley *et al.* [16], respectively. Error bars shown only if larger than the symbol denoting the experiment.

the same set of states as at 10 eV. Using Eq. (57) we also combined the measurements at 10 eV, presented in Fig. 3, to compare the results of two independent groups. We see that they are in very good agreement with each other, and we are also able to distinguish between the three theories in favor of CCC. Comparison of CC with the other theories and experiment shows that these measurements can only be reproduced with the inclusion of the target continuum. Though CCO does very well in reproducing the measurements it is once more clear that CCC is better.

Our presentation of electron-sodium scattering would not be complete without looking at differential cross sections. In Figs. 9 and 10 we present, respectively, the elastic and inelastic $3P$ differential cross sections at 10, 20, 22.1, and 54.4 eV. The CCC results were generated from the calculations described above at corresponding energies. For purposes of graphic presentation we normalized the measurements to our theory at the forward scattering angles, with the integrated cross sections given in Table II. There is little to distinguish between the three theories, indicating that differential cross sections are predominantly influenced by the inclusion of the first few discrete eigenstates. Variation between different sets of measurements is much greater than that between the theories, indicating the difficulty associated with measuring cross sections as they vary many orders of magnitude from forward to backward angles. As such it is clear that differential cross sections are much less sensitive to the

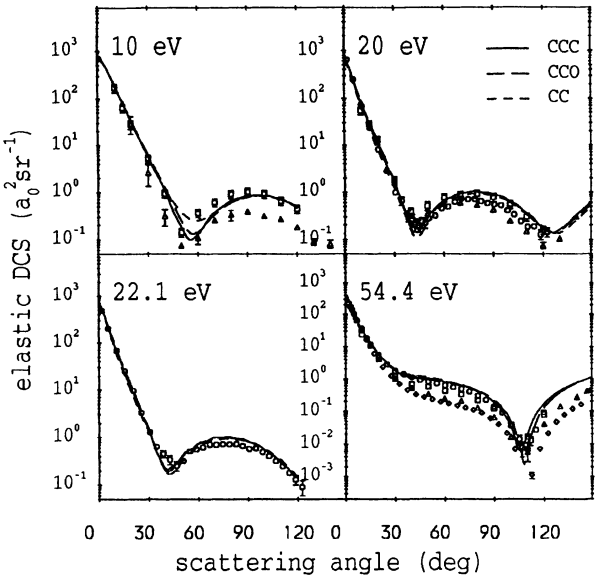

FIG. 9. Elastic electron-sodium differential cross sections at projectile energies of 10, 20, 22.1, and 54.4 eV. The CCC results were generated using the same sets as specified in Figs. 1, 3, 4, and 7. The CCO and CC theories are as in Fig. 1. The experiments of Lorentz and Miller [57] are denoted by ○. Those of Srivastava and Vušković [52] are denoted by □. The measurements of Allen *et al.* [58] are denoted by ◇. The most recent results of Marinković *et al.* [59] are denoted by △. All measurements have been normalized to the theory. Error bars are only plotted if they are larger than the size of the symbol denoting the experiment.

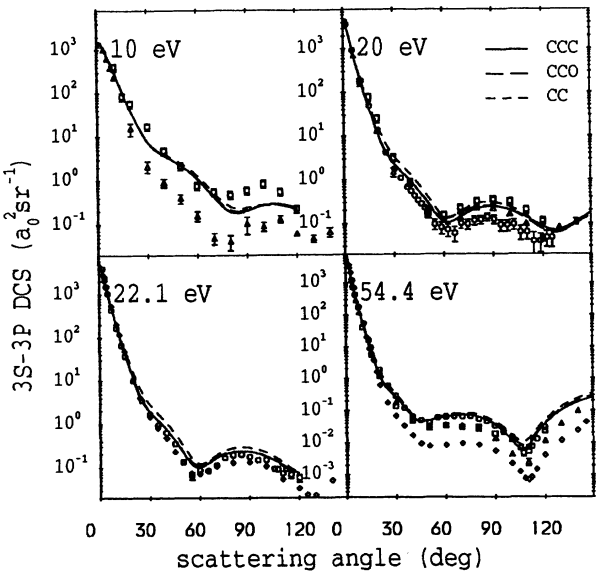

FIG. 10. Inelastic ($3\,^2S - 3\,^2P$) electron-sodium differential cross sections at projectile energies of 10, 20, 22.1, and 54.4 eV. The theoretical and experimental results are as in Fig. 9. The measurements denoted by ◇ are from Refs. [60] and [61].

detail of theory and are not as useful for the testing of theory as are the accurate spin-resolved "ratio" measurements presented in Figs. 1–8.

Having presented most of our results in pictorial form, we now look quantitatively at the resulting various integrated and total cross sections. It is these types of quantities that are of practical importance in many fields of research. It is of primary motivation to us to be able to calculate these accurately. We use the detailed data above to test the theory which in turn gives us confidence in the claim that we are able to present reliable integrated results. In Table II we present integrated cross sections for electron scattering on the ground state of sodium for states with principle quantum number $n \leq 4$ and orbital angular momentum $l \leq 3$. We do not expect the level of accuracy to be the same for each state. For example, given that we do not include $l = 4$ states in the CCC calculation the $4f$ has not been checked for convergence with increasing l. Total and total ionization cross sections, as well as total ionization spin asymmetry, are also presented and compared with experiment wherever possible.

Though there is quite a good deal of experimental data for the integrated cross sections, most of it has rather large error bars and is in good agreement with our results. On occasion when two conflicting experiments are available, the theory agrees with one better than the other. However, there is a particular systematic exception that is worth discussing. Our result for the total ionization cross section, which is essentially derived by summing the integrated cross sections for states with positive energies [11], is consistently almost a factor of 2 less than the experiments, performed in the 1960s, of Zapesochnyi and Aleksakhin [48] and McFarland and Kinney [49]. Yet the corresponding spin asymmetry is in excellent agreement with the much more recent measurements of Baum *et al.* [50]. Given this fact, as well as the excellent quantitative agreement with experiment for both of these observables in e-H scattering [11], it is our hope that our total ionization cross section results for sodium are equally good.

IV. CONCLUSIONS

We have generalized the convergent close-coupling formalism for e-H scattering of Bray and Stelbovics [1] to hydrogenlike atoms Li, Na, K, and ions such as He^+, Li^{2+}, Be^+, Ar^{7+}, etc. This was achieved by treating the scattering system on these targets as a three-body problem of two electrons moving in the Hartree-Fock potential of the frozen core. The target states are obtained by diagonalizing the target Hamiltonian in a large Laguerre basis. The projectile is expanded in a set of distorted (distorted Coulomb for ions) waves with allowance for an arbitrary number of bound states arising from the distorting potential. Correct symmetrization is ensured throughout. In the two-electron potential matrix elements at least one electron is represented by a square-integrable function, and so at most one of these may be a true continuum function, ensuring that all potential matrix elements exist. This allows for the application of the method to

TABLE II. Integrated (σ_{nl}), total ionization (σ_i), and total (σ_t) cross sections in units of πa_0^2, as well as total ionization spin asymmetry (A_i), for electron scattering on the ground state of sodium at a range of energies calculated using the CCC method. The experimental data of Srivastava and Vušković [52] are denoted by σ_{ns}^a, those of Enemark and Gallagher [53] by σ_{3p}^b, those of Phelps and Lin [54] by σ_{nl}^c, those of Kwan *et al.* [55] by σ_t^f, and those of Kasdan, Miller, and Bederson [56] by σ_t^g. The total ionization cross section measurements by Zapesochnyi and Aleksakhin [48] and McFarland and Kinney [49] are denoted by σ_i^d. The measurements of the total ionization spin asymmetry by Baum *et al.* [50] are denoted by A_i^e. Cubic spline interpolation has been used when required. Spin and magnetic sublevel dependent quantities may be obtained by correspondence with the author.

E (eV)	4.1	10.0	20.0	40.0	54.4
σ_{3s}	62.4	22.3	11.9	7.62	6.35
σ_{3s}^a		48.9±14.7	15.9±4.8	12.5±3.8	6.14±1.84
σ_{3p}	32.5	35.3	32.2	24.6	20.6
σ_{3p}^b	35.6±1.0	36.5±1.6	32.9±1.1	25.2±0.7	21.4±0.5
σ_{3p}^c		40.5±4.8	36.1±4.3	28.3±3.4	24.2±2.9
σ_{3d}	3.67	3.53	2.81	1.67	1.25
σ_{3d}^c		4.17±0.63	2.67±0.40	1.55±0.23	1.13±0.17
σ_{4s}	1.26	0.84	0.76	0.53	0.43
σ_{4s}^a		1.14±0.34	0.59±0.18	0.66±0.20	0.34±0.10
σ_{4s}^c		1.10±0.44	0.93±0.37	0.74±0.29	0.62±0.25
σ_{4p}	1.41	1.00	0.85	0.66	0.55
σ_{4p}^c		0.66±0.27	0.66±0.27	0.51±0.20	0.42±0.17
σ_{4d}		0.78	0.74	0.49	0.34
σ_{4d}^c		0.96±0.19	0.63±0.13	0.38±0.08	0.28±0.06
σ_{4f}		0.42	0.23	0.08	0.06
σ_i		4.42	4.65	3.12	2.54
σ_i^d		7.16	7.39	5.91	5.34
A_i		0.41	0.28	0.18	0.14
A_i^e		0.45±0.02	0.30±0.02	0.21±0.02	0.16±0.02
σ_t	101.2	70.9	55.0	39.7	32.8
σ_t^f	76.2±16.0	65.3±13.7	50.1±10.5	34.4±7.2	28.2±5.9
σ_t^g	104.5±12.5	85.2±10.2	73.9±8.9	68.2±8.2	

all partial waves and projectile energies, and reduces the problem of calculating electron-hydrogenlike target scattering to being able to achieve convergence as a function of increasing the number of states in the close-coupling formalism.

We have demonstrated the utility of the method by applying it to electron scattering on the ground state of atomic sodium. The method has been applied to the extensive set of measurements available at an energy range of 1–54.4 eV with which we generally find excellent quantitative agreement. It is particularly pleasing to have found excellent agreement with the same parameters for which agreement is quite poor in the simpler electron-hydrogen scattering system.

We have been able to establish convergence for the transitions involving the ground state and the first excited state at projectile energies above the ionization threshold by the use of just those target states that lead to open channels. This conclusion must be seen as transition and target dependent. In general, we establish convergence by performing a number of calculations with ever increasing number of states, until convergence is obtained. This does make the assumption that any further increase, no matter how large, in the number of states used will not result in a significant change in the observables of interest.

The only other theory, that we are aware of, which is able to perform almost as well over the entire energy range of 1–54.4 eV is the CCO method of Bray and McCarthy [28]. Though this method is able to treat more target partial waves using our computational facilities than does the CCC method, we have found that it is more important to treat the lower partial waves of the continuum states more accurately than to treat a larger number of them. The singlet $L_\perp$ parameter at 10 eV indicates that it is very important to treat the continuum very accurately in order to be always sure that the full set of scattering amplitudes is calculated reliably. Only the CCC method is able to do this.

It now remains to apply the method to scattering from excited states, e.g., look at nP-nD transitions where initial investigations show that convergence may be considerably more difficult to obtain. This, however, would be a reflection on the complexity of the problem rather than the utility of the CCC method. Initial application of the method to the $2s$, $2p$, and total ionization cross sections in e-He^+ scattering is yielding very promising results. We also intend to expand the method further to apply it to e-$2e$ processes and the "four-body" problem of e-He scattering. This work is currently under way.

ACKNOWLEDGMENTS

The author would like to thank Dmitry Fursa, Ian McCarthy, Andris Stelbovics, Peter Teubner, and David Norcross for a number of useful discussions. The free use of the LAPACK set of routines [40] is gratefully acknowledged. The author would also like to thank Barry Schneider and Bob McEachran for very helpful correspondence, and Friedrich Hanne and Günter Baum for providing their data in quantitative form. I also thank The Flinders University of South Australia and the Australian Research Council in providing a SUN SS10/512 workstation in pursuit of progress in this project.

[1] I. Bray and A. T. Stelbovics, Phys. Rev. A **46**, 6995 (1992).
[2] T. T. Scholz, H. R. J. Walters, P. G. Burke, and M. P. Scott, J. Phys. B **24**, 2097 (1991).
[3] J. Callaway, Phys. Rev. A **32**, 775 (1985).
[4] W. L. van Wyngaarden and H. R. J. Walters, J. Phys. B **19**, 929 (1986).
[5] D. H. Madison, I. Bray, and I. E. McCarthy, J. Phys. B **24**, 3861 (1991).
[6] I. Bray, D. A. Konovalov, and I. E. McCarthy, Phys. Rev. A **44**, 5586 (1991).
[7] R. Poet, J. Phys. B **11**, 3081 (1978).
[8] A. Temkin, Phys. Rev. **126**, 130 (1962).
[9] I. Bray and A. T. Stelbovics, Phys. Rev. Lett. **69**, 53 (1992).
[10] I. Bray and A. T. Stelbovics, At. Data Nucl. Data Tables (to be published).
[11] I. Bray and A. T. Stelbovics, Phys. Rev. Lett. **70**, 746 (1993).
[12] B. Bedereson, Comments At. Mol. Phys. **1**, 41 (1969).
[13] J. J. McClelland, M. H. Kelley, and R. J. Celotta, Phys. Rev. A **40**, 2321 (1989).
[14] J. J. McClelland, S. R. Lorentz, R. E. Scholten, M. H. Kelley, and R. J. Celotta, Phys. Rev. A **46**, 6079 (1992).
[15] R. E. Scholten, S. R. Lorentz, J. J. McClelland, M. H. Kelley, and R. J. Celotta, J. Phys. B **24**, L653 (1991).
[16] M. H. Kelley, J. J. McClelland, S. R. Lorentz, R. E. Scholten, and R. J. Celotta, in *Correlations and Polarization in Electronic and Atomic Collisions and (e,2e) Reactions*, edited by P. J. O. Teubner and E. Weigold, IOP Conf. Proc. No. 122 (Institute of Physics and Physical Society, London, 1992), p. 23.
[17] S. R. Lorentz, R. E. Scholten, J. J. McClelland, M. H. Kelley, and R. J. Celotta, Phys. Rev. Lett. **67**, 3761 (1991).
[18] D. L. Moores and D. W. Norcross, J. Phys. B **5**, 1482 (1972).
[19] J. Mitroy, I. E. McCarthy, and A. T. Stelbovics, J. Phys. B **20**, 4827 (1987).
[20] D. H. Madison, K. Bartschat, and R. P. McEachran, J. Phys. B **25**, 5199 (1992).
[21] I. E. McCarthy, J. Mitroy, and R. Nicholson, J. Phys. B **24**, L449 (1991).
[22] I. Bray, Phys. Rev. Lett. **69**, 1908 (1992).
[23] I. Bray, Z. Phys. D (to be published).
[24] I. Bray, Phys. Rev. A **49**, R1 (1994).
[25] I. E. McCarthy and A. T. Stelbovics, Phys. Rev. A **28**, 2693 (1983).
[26] I. Bray, I. E. McCarthy, J. Mitroy, and K. Ratnavelu, Phys. Rev. A **39**, 4998 (1989).
[27] I. Bray, D. A. Konovalov, and I. E. McCarthy, Phys. Rev. A **43**, 5878 (1991).
[28] I. Bray and I. E. McCarthy, Phys. Rev. A **47**, 317 (1993).
[29] L. V. Chernysheva, N. A. Cherepkov, and V. Radojevic, Comput. Phys. Commun. **11**, 57 (1976).
[30] R. P. McEachran and M. Cohen, J. Phys. B **16**, 3125 (1983).
[31] H. L. Zhou, B. L. Whitten, G. Snitchler, D. W. Norcross, and J. Mitroy, Phys. Rev. A **42**, 3907 (1990).
[32] R. P. McEachran, A. D. Stauffer, and S. Greita, J. Phys. B **12**, 3119 (1979).
[33] I. Bray, D. V. Fursa, and I. E. McCarthy, Phys. Rev. A **47**, 3951 (1993).
[34] H. A. Yamani and W. P. Reinhardt, Phys. Rev. A **11** 1144 (1975).
[35] A. T. Stelbovics, J. Phys. B **22**, L159 (1989).
[36] I. Bray and A. T. Stelbovics, Phys. Rev. A **48**, 4787 (1993).
[37] A. T. Stelbovics, Phys. Rev. A **41**, 2536 (1990).
[38] M. Gell-Mann and M. L. Goldberger, Phys. Rev. **91**, 398 (1953).
[39] B. H. Bransden, C. J. Noble, and R. N. Hewitt, J. Phys. B **26**, 2487 (1993).
[40] E. Anderson, Z. Bai, C. Bischof, J. Demmel, J. Dongarra, J. Du Croz, A. Greenbaum, S. Hammarling, A. McKenney, S. Ostrouchov, and D. Sorensen, *LAPACK User's Guide* (Society for Industrial and Applied Mathematics, Philadelphia, 1992).
[41] B. I. Schneider and L. A. Collins, Comput. Phys. Commun. **53**, 381 (1989).
[42] N. Andersen, J. W. Gallagher, and I. V. Hertel, Phys. Rep. **165**, 1 (1988).
[43] N. Andersen and K. Bartschat, Comments At. Mol. Phys. (to be published).
[44] V. Nickich, T. Hegemann, M. Bartsch, and G. F. Hanne, Z. Phys. D **16**, 261 (1990).
[45] H. L. Zhou, D. W. Norcross, and B. L. Whitten, *Correlations and Polarization in Electronic and Atomic Collisions and (e,2e) Reactions* (Ref. [16]).
[46] R. E. Scholten, G. F. Shen, and P. J. O. Teubner, J. Phys. B **26**, 987 (1993).
[47] R. T. Sang, P. M. Farrell, D. H. Madison, W. R. MacGillivray, and M. C. Standage (unpublished).
[48] I. P. Zapesochnyi and I. S. Aleksakhin, Zh. Eksp. Teor. Fiz. **55**, 76 (1968) [Sov. Phys.—JETP **28**, 41 (1969)].
[49] R. H. McFarland and J. D. Kinney, Phys. Rev. **137**, A1058 (1965).
[50] G. Baum, M. Moede, W. Raith, and W. Schröder, J. Phys. B **18**, 531 (1985).
[51] C. E. Moore, *Atomic Energy Levels*, Natl. Bur. Stand.

(U.S.) Circ. No. 467 (U.S. GPO, Washington, DC, 1949), Vol. 1.
[52] S. K. Srivastava and L. Vušković, J. Phys. B **13**, 2633 (1980).
[53] E. A. Enemark and A. Gallagher, Phys. Rev. A **6**, 192 (1972).
[54] J. O. Phelps and C. C. Lin, Phys. Rev. A **24**, 1299 (1981).
[55] C. K. Kwan, W. E. Kauppila, R. A. Lukaszew, S. P. Parikh, T. S. Stein, Y. J. Wan, and M. S. Dababneh, Phys. Rev. A **44**, 1620 (1991).
[56] A. Kasdan, T. M. Miller, and B. Bederson, Phys. Rev. A **8**, 1562 (1973).
[57] Steven R. Lorentz and Thomas M. Miller (unpublished).
[58] L. J. Allen, M. J. Brunger, I. E. McCarthy, and P. J. O. Teubner, J. Phys. B **20**, 4861 (1987).
[59] B. Marinković, V. Pejčev, D. Filipović, I. Čadež, and L. Vušković, J. Phys. B **25**, 5179 (1992).
[60] P. J. O. Teubner, J. L. Riley, M. J. Brunger, and S. J. Buckman, J. Phys. B **19**, 3313 (1986).
[61] S. J. Buckman and P. J. O. Teubner, J. Phys. B **12**, 1741 (1979).